

Microstructure and Properties of Carbon Block Refractories Containing Thermally Oxidized Anthracite for Blast Furnaces

T. Wang, S. Sang*, Y. Li, Y. Xu, Q. Wang

The State Key Laboratory of Refractories and Metallurgy, Wuhan University of Science and Technology, Wuhan 430081, PR China

received October 10, 2017; received in revised form November 23, 2017; accepted December 4, 2017

Abstract

Carbon block refractories containing thermally oxidized anthracite (TOA) and additives of Al and Si were prepared for use in blast furnaces. The TOA was obtained by treating electrically calcined anthracite (ECA) using the thermal oxidation method. It was then introduced into carbon blocks by partially or totally replacing the ECA raw materials. The microstructure and properties of carbon block refractories heated in a coke bed at 1400 °C were investigated. The results revealed that TOA accelerated the formation of β -SiC whiskers and β -Sialon phases in carbon block refractories because TOA has higher reactivity than ECA. Properties such as the cold compressive strength, mean pore diameter, < 1 μ m pore volume ratio and thermal conductivity of carbon block refractories with TOA were improved remarkably compared with those without TOA. It was suggested that the *in-situ*-formed ceramic phases in the matrix and on the aggregates both had a strengthening effect on the carbon block refractories. Moreover, the whiskers formed in the matrix were more favorable for forming an excellent microporosity structure as they filled the pores while the whiskers on the aggregates were more beneficial for reducing the interface thermal resistance between the aggregates and matrix, thus promoting the thermal conductivity of the carbon block refractories.

Keywords: Thermally oxidized anthracite, microstructure, thermal conductivity, carbon block refractories

I. Introduction

Carbon block refractories based on electrically calcined anthracite (ECA) have been widely used in ironmaking industries as working linings for blast furnaces owing to their superior resistance to molten iron and excellent alkali resistance¹⁻². However, with the development of higher smelting intensity technologies for blast furnaces³, traditional ECA-based carbon block refractories, which have low thermal conductivity and poor microporosity structures, can no longer meet the requirements of those technologies. Therefore, it is essential to develop carbon block refractories with better performance, such as higher thermal conductivity, better microporosity structures and molten iron resistance⁴⁻⁵. Silicon and aluminum additives are commonly added to carbon block refractories to enhance their performance based on *in-situ*-forming ceramic phases such as SiC, AlN, Al₃C₄ and Al₄SiC₄, etc.⁶⁻⁷. On the one hand, the ceramic phases can fill the pores and gaps in the matrix to decrease the pore size and optimize the matrix structure. On the other hand, these *in-situ* ceramic phases possess high thermal conductivity, which can construct a highly conductive network to improve the thermal conductivity of carbon block refractories. Chen *et al.*⁸ reported that the addition of silicon in combination with aluminum promoted the performance of carbon block refractories owing to the formation of lots of well-developed SiC and AlN whiskers.

Actually, many studies on promoting the formation of *in-situ* ceramic phases and optimizing their morphologies have been conducted to further enhance the mechanical and thermal properties of carbon-containing refractories. These mainly include the use of an appropriate amount of additives with a suitable particle size⁹⁻¹⁰, decreasing the partial pressure of oxygen^{7,11}, the addition of silicates¹²⁻¹³ or the use of active carbon sources such as carbon black, carbon nanotubes (CNTs), expanded graphite and graphene nanosheet, etc.¹⁴⁻¹⁶. Li *et al.*¹⁷ found that the addition of CNTs benefited *in-situ* formation of well-developed SiC whiskers in the matrix, and consequently the thermal conductivity of the carbon block refractories was improved. The literature¹⁸⁻²⁰ reported that better mechanical and thermo-mechanical properties of low-carbon MgO-C and Al₂O₃-C refractories could be obtained when expanded graphite or graphene nanosheet was added because those active carbon sources accelerated the *in-situ* formation of ceramic phases in the specimens owing to their higher reactivity.

In fact, ECA is also promising as an active carbon source. ECA is a low-crystalline carbon material that is capable of being graphitized in high-temperature treatment²¹⁻²⁴. And according to our previous study²⁵, reactive graphite with many more defects could be obtained by treating natural graphite flake with the thermal oxidation method, which was able to accelerate the formation of SiC whiskers when the graphite was mixed with silicon powder and

* Corresponding author: sangshaobai@126.com

heated in the coke bed. If ECA were to be treated with the thermal oxidation method, the surface amorphous carbon of ECA might be eliminated and graphitized carbon on the ECA surface would be exposed. On the other hand, plenty of defects could form in surface-graphitized carbon, as the activated carbon spots can react with Si sources to form SiC. The ECA could act as an active carbon source after treatment with the thermal oxidation method and then accelerate the formation of SiC whiskers, thus improving the performance of carbon block refractories. Hence, the evolution of microstructure and performance of carbon block refractories with the addition of thermally oxidized anthracite (TOA) and additives of Al and Si during heat treatment were investigated in the present work.

II. Experimental

(1) Preparation of thermally oxidized anthracite (TOA)

In the experiment, TOA was prepared by treating ECA with the thermal oxidation method. Namely, the ECA aggregates (5–3 mm or 3–1 mm or 1–0 mm, >85% C, Lushan, China) or fine powder (74 μm , >85% C, Lushan, China) were put into an iron saggars. The volume of ECA materials accounted for about one third of the volume of the iron saggars. The iron saggars was covered with a lid to make sure no air could get into the saggars. Then, the whole saggars was put into an electric furnace and heated from room temperature to 1000 °C at a heating rate of 5 K/min. The holding time at the final temperature was 6 h. A simple schematic diagram of the thermal oxidation treatment for ECA is shown in Fig. 1.

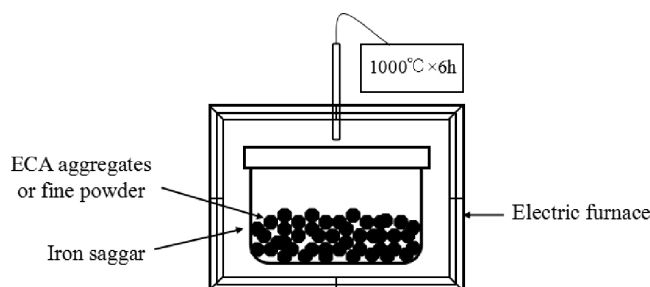


Fig. 1: A simple schematic diagram of thermal oxidation treatment for ECA.

(2) Preparation of carbon block refractories specimens

ECA aggregates and fine powder, $\alpha\text{-Al}_2\text{O}_3$ powder (2 μm , 99 wt% Al_2O_3 , Kaifeng, China), Si powder (45 μm , 98.5 wt% Si, Wuhan, China) and Al powder (88 μm , 99 wt% Al, Wuhan, China) were used as raw materials. Thermosetting phenolic resin (liquid, >40% fixed carbon; Wuhan, China) was used as a binder. The batch containing 82 wt% ECA, 6 wt% $\alpha\text{-Al}_2\text{O}_3$ powder, 10 wt% Si powder and 2 wt% Al powder was a basis batch composition, denoted as ECA-R. On the basis of ECA-R, the specimens in which the ECA aggregates and ECA powder were replaced with TOA aggregates (5–3 mm, 3–1 mm and 1–0 mm) and TOA powder (<0.074 mm) were designated as TOA-A and TOA-M, respectively. And the batch in which all the ECA in ECA-R was substituted by TOA was denoted as TOA-AM. The batch compositions of all investigated carbon block refractories are listed in Table 1.

All the raw materials were mixed for about 30 min in the mixer with the rotation rate of 80–120 rpm. After kneading, cylindrical specimens measuring 50 mm in diameter and 50 mm in height were cold pressed under the pressure of 100 MPa and cured at 110 °C for 24 h. Then, the carbon block refractories specimens were embedded in coke powder in an alumina saggars and heated from room temperature to 1400 °C at a heating rate of 5 K/min. The soaking time at the final temperature was 3 h.

(3) Testing and characterization methods

The phase compositions were analyzed by means of X-ray diffraction (XRD, Philips X' Pert Pro; Philips, Amsterdam, Netherlands), using Ni-filtered $\text{CuK}\alpha$ radiation at a scanning speed of 2 deg/min. The microstructure of carbon block refractories as well as anthracite aggregates was investigated by means of scanning electron microscopy (Nova400 Nano SEM; FEI Company, Hillsboro, OR) linked with energy-dispersive X-ray spectroscopy (EDS; Phoenix EDS Microanalysis system; EDAX, Inc., Mahwah, NJ). Meanwhile, thermogravimetric differential scanning calorimetry (TG-DSC, STA499, NETZSCH, Germany) was employed to evaluate the reactivity and calculate the non-isothermal oxidation kinetics of the ECA and TOA raw materials. The bulk density and apparent porosity of the carbon block refractories were measured according to the Archimedes' principle. The pore size distribution was determined by means of mercury porosimetry (Autopore IV9500; Micromeritics Instrument Corp., Norcross, GA). The cold compressive strength was measured according to GB/T 5072–2008. Thermal conductivity was measured with a laser thermal conductivity meter (Flashline 5000; AnterCorp., Penn Hills, PA) from cylindrical samples measuring 12.5 mm in diameter and 2.5–3.0 mm in thickness.

III. Results and Discussion

(1) Phase composition

The phase composition of all specimens fired at 1400 °C are examined and shown in Fig. 2. For specimen ECA-R, corundum and graphite were detected as raw materials, Si and Al disappeared completely whereas $\beta\text{-SiC}$ and $\beta\text{-Sialon}$ were formed due to *in-situ* reaction of Si and Al in reducing atmosphere²⁶. With regard to the specimens containing TOA, no new crystallographic phase formed but the diffraction peak intensity of graphite, $\beta\text{-SiC}$ and $\beta\text{-Sialon}$ phases was much stronger than that of specimen ECA-R. And the peak intensity of $\beta\text{-SiC}$ in specimen TOA-M was a little higher than that of specimen TOA-A. It was obvious that in specimen TOA-AM, the diffraction peak intensity of graphite, $\beta\text{-SiC}$ and $\beta\text{-Sialon}$ was the highest among all the specimens. The above phase composition evolutions demonstrated that the addition of TOA accelerated the formation of SiC and Sialon phases in the specimens.

Table 1: Compositions of the investigated carbon refractories.

Ingredient (wt%)	ECA-R	TOA-A	TOA-M	TOA-AM
ECA aggregates	68		68	
ECA powder	14	14		
As-received TOA aggregates		68		68
As-received TOA powder			14	14
α -Al ₂ O ₃ powder	6	6	6	6
Al powder	2	2	2	2
Si powder	10	10	10	10
Phenolic resin	+15	+15	+15	+15

Table 2: Properties of carbon refractories specimens fired at 1673 K (1400 °C).

Properties	ECA-R	TOA-A	TOA-M	TOA-AM
BD (g/cm ³)	1.70	1.71	1.70	1.69
AP (pct)	14.7±0.1	15.2±0.1	14.4±0.1	15.0±0.1
CCS (MPa)	23.6±0.4	37.2±2.9	37.1±1.6	37.0±0.3
Mean Pore Diameter (nm)	228.7	180.6	133.0	120.9
< 1 μ m Pore Volume Ratio (pct)	73.40	78.38	81.17	86.55
TC (W·m ⁻¹ ·K ⁻¹) (25 °C)	6.28	11.60	8.17	18.40

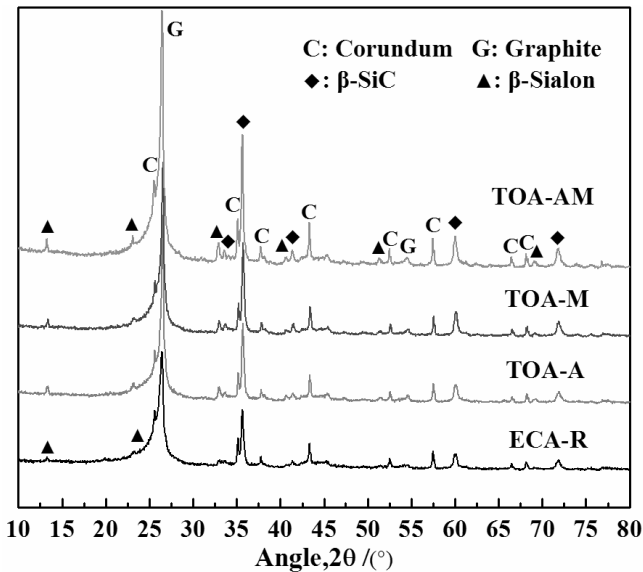


Fig. 2: XRD pattern of the specimens fired at 1673 K (1400 °C).

(2) Microstructure

The microstructure of all specimens coked at 1400 °C are shown in Fig. 3. As for specimen ECA-R, only a few β-SiC whiskers (identified by means of XRD and EDS analysis) were found in the matrix (Fig. 2a) and a small part of the β-SiC whiskers twisted and joined with each other (Fig. 2b). With regard to specimens containing TOA, β-SiC whiskers were much more easily found compared to specimen ECA-R. It was worth noting that the matrix structure in specimen TOA-A and TOA-M was different. The β-SiC whiskers were located on the aggregates in specimen TOA-A (Fig. 2c and 2d) while β-SiC whiskers mainly appeared in the matrix in specimen TOA-M (Fig. 2e and 2f). For specimen TOA-AM, not only a number of well-

developed β-SiC whiskers could be observed in the matrix (Fig. 2g), but a large number of needle-like β-Sialon phases (confirmed with XRD and EDS analysis) was found on the aggregates, too (Fig. 2h). Besides, β-SiC whiskers also appeared on the aggregates in specimen TOA-AM, which interlocked with the whiskers in the matrix to fill the pores between aggregates and matrix (Fig. 2i and 2j), implying that specimen TOA-AM might have better microporosity structure.

(3) Properties of carbon block refractories specimens

The properties of all specimens such as bulk density (BD), apparent porosity (AP), cold compressive strength (CCS), mean pore diameter, < 1 μ m pore volume ratio and thermal conductivity (TC) were measured and the results are presented in Table 2. The CCS and TC of specimens containing TOA were improved significantly compared to specimen ECA-R. For example, the CCS and TC of specimen ECA-R at 1400 °C were 23.6 MPa and 6.28 W·m⁻¹·K⁻¹, which were increased to 37.2 MPa and 11.60 W·m⁻¹·K⁻¹ for specimen TOA-A, respectively. In addition, the properties of specimen TOA-A and TOA-M were a little different. For example, specimen TOA-A exhibited higher TC than specimen TOA-M while specimen TOA-M showed much lower mean pore diameter and higher < 1 μ m pore volume ratio than specimen TOA-A, which might be related to the different matrix microstructure of the specimens. As shown in SEM micrographs, many β-SiC whiskers were observed on the aggregates in specimen TOA-A (Fig. 2c and 2d), which reduced the interface thermal resistance and subsequently improved the TC of specimens. However, lots of β-SiC whiskers

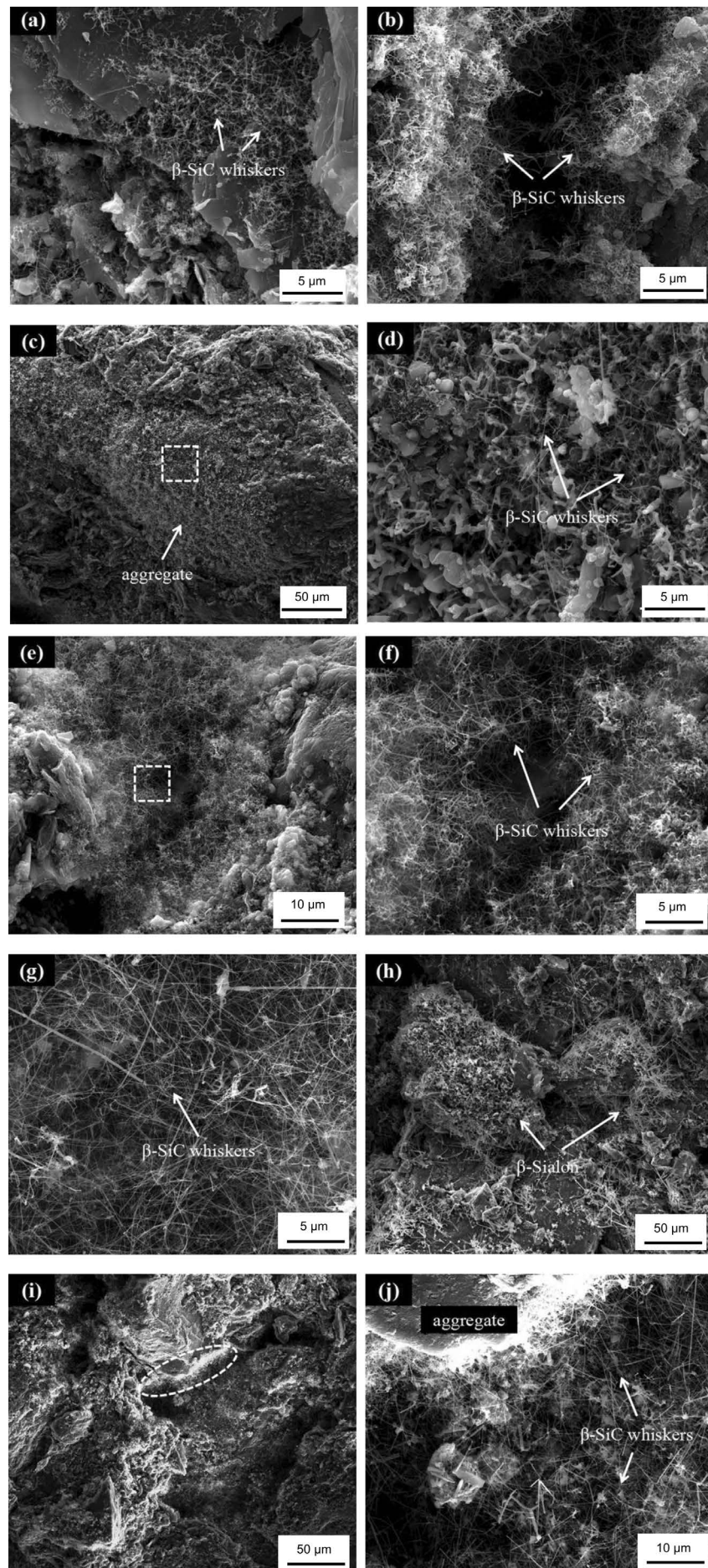


Fig. 3: SEM micrographs of specimens cured at 1673 K (1400 °C): (a)-(b) ECA-R, (c)-(d) TOA-A, (e)-(f) TOA-M and (g)-(j) TOA-AM.

with a high length-diameter ratio appeared in the matrix in specimen TOA-M (Fig. 2e and 2f), which interlocked with each other to form inter-textures and thus contributed to promoting the microporosity characteristics. It is notable that the specimen TOA-AM had the lowest mean pore diameter and the highest $< 1 \mu\text{m}$ pore volume ratio and TC at 1400°C owing to the joint efforts of ceramic phases both on the aggregates and in the matrix, the mean pore diameter decreased to 120.9 nm , $< 1 \mu\text{m}$ pore volume ratio was improved to 86.55% , and TC was increased to $18.40 \text{ W}\cdot\text{m}^{-1}\cdot\text{K}^{-1}$.

(4) Discussion

Based on the results presented above, it could be concluded that the phase composition, microstructure and properties of carbon block refractories were influenced by the addition of TOA. The XRD pattern demonstrated that the TOA promoted the formation of *in-situ* ceramic phases, which might be attributed to the higher reactivity of TOA. Additionally, the SEM micrographs showed that there is little difference in the matrix structure for specimens TOA-A and TOA-M. The $\beta\text{-SiC}$ whiskers located on the aggregates in specimen TOA-A with addition of TOA aggregates (Fig. 2c and 2d), while $\beta\text{-SiC}$ whiskers mainly appeared in the matrix in specimen TOA-M with addition of TOA powder (Fig. 2e and 2f), which suggested the location of ceramic whiskers was strongly dependent on the TOA raw materials.

Raman spectrum analysis was conducted to characterize the graphitization degree of ECA and TOA. As shown in Fig. 4, two peaks are detected in the Raman spectrum for all anthracites. One appearing in the $1300\text{--}1400 \text{ cm}^{-1}$ spectral region is known as D band (D for disorder) and the other one appearing in the $1550\text{--}1650 \text{ cm}^{-1}$ spectral region is G band (G for graphite). For ECA powder, weak D and G peaks can be observed, indicating lots of amorphous carbon and few structural defects existing in ECA²⁷. With thermal activation of the ECA, the intensity of D and G peaks both increased aggressively, manifesting the presence of more crystallized graphite and structural defects in TOA. The existence of structural defects in the carbon source corresponds to fractured C=C bonds, which are the source of activated carbon atoms that can react with Si sources to form SiC in a reducing atmosphere²⁵. Based on the above results of XRD and Raman spectrum analysis, it could be confirmed that the graphitization degree of ECA was promoted by the thermal oxidation method and the reactivity might be improved as well.

With regard to the reactivity of ECA and TOA powder, non-isothermal kinetics, both Kissinger and Ozawa methods^{28–29}, were employed in the present work to estimate the activation energy for ECA and TOA powder. Calorimetric signals of phase transformation were recorded in DSC analysis when the samples were continuously heated from room temperature to 1200°C in air atmosphere at a heating rate of $5\text{--}20 \text{ K/min}$. Fig. 5 shows the heating rate dependence of DSC curves for ECA and TOA powder. It could be observed that the exothermic oxidation peak of TOA powder is a little sharper and the temperature is a little higher compared with ECA powder at the same heating rate.

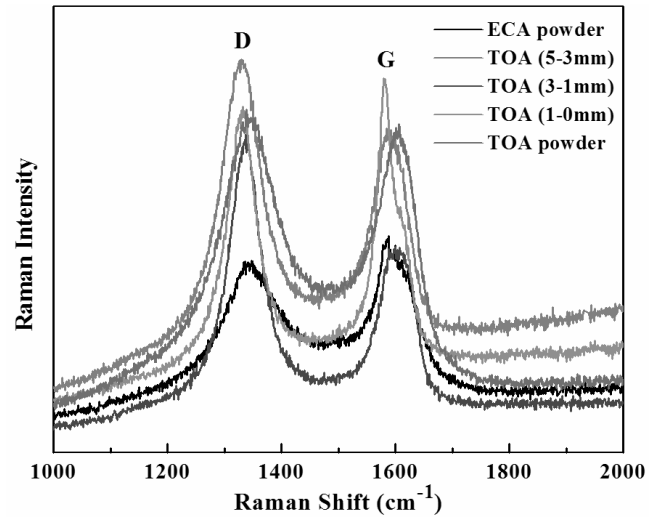


Fig. 4: Raman spectrum of anthracite aggregates and powder.

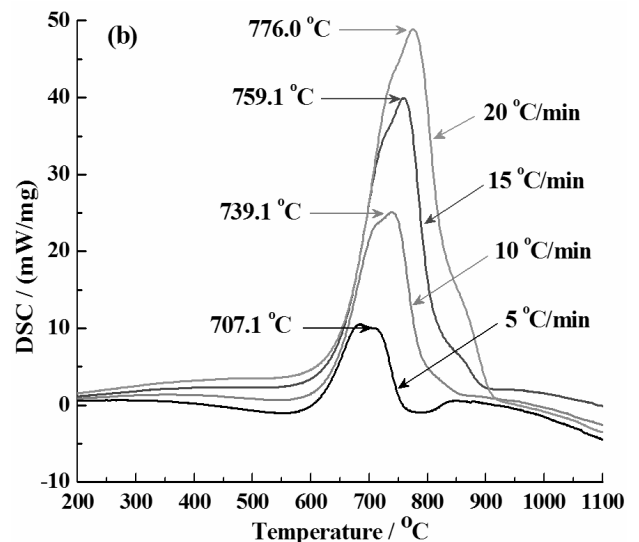
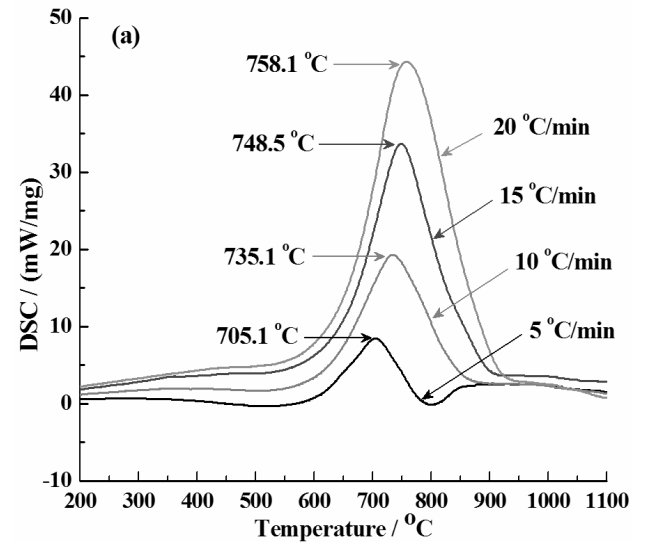


Fig. 5: DSC curves for ECA powder (a) and TOA powder (b) with various heating rates.

The oxidation activation energy calculated from the Kissinger and Ozawa plots is presented in Table 3. It was found that the oxidation activation energy of ECA and TOA powder deduced from the slopes of the Kissinger and Ozawa plots is similar. The oxidation activation energies of ECA powder are 200.44 kJ/mol and 206.47 kJ/mol. However, the oxidation activation energies of TOA powder are lower than that of ECA powder, which indicated that TOA powder has higher reactivity than that of ECA powder. So, the addition of TOA with higher reactivity to carbon block refractories accelerated the formation of ceramic phases, which resulted in better properties of the specimens containing TOA.

An additional experiment was also conducted to better prove that TOA can react with silicon to form SiC whiskers. A certain amount of ECA and TOA aggregates (5–3 mm was chosen in this work) was put into an alumina crucible with the same amount of silicon in the bottom, respectively, and there was no direct contact between the anthracite aggregates and silicon powder. The alumina crucible then was fired in a coke bed at 1200 °C for 3 h. The SEM micrographs of ECA and TOA aggregates fired at 1200 °C with silicon are shown in Fig. 6. It could be clearly seen that only a few β -SiC whiskers were observed separately on the ECA aggregates (Fig. 6a). However, on the TOA aggregates, a large number of β -SiC whiskers was found, and the TOA aggregates were even totally covered by well-crystallized β -SiC whiskers (Fig. 6b). The result strongly indicated that TOA with higher reactivity could react with Si sources (such as Si_(g) or SiO_(g)) to form β -SiC whiskers.

Table 3: The oxidation activation energies (kJ/mol) of ECA and TOA powder in air.

Methods	ECA powder	TOA powder
Kissinger	200.44	156.34
Ozawa	206.47	164.69

It could be concluded that TOA with higher reactivity could be obtained with the thermal oxidation method and a special layered structure similar to a core-shell structure was formed in TOA. A simple schematic illustration of the formation of the core-shell structure in TOA is presented in Fig. 7. After treatment with the thermal oxidation method, the surface amorphous carbon in ECA could be eliminated and the graphitized carbon shell exposed³⁰. The inner part, also called the core, in TOA remained the same as that in ECA because the air is limited during the thermal oxidation treatment. Furthermore, it was worth noting that many defects were formed in the graphitized carbon shell of TOA during thermal oxidation treatment, which was because the activated carbon spots can react with Si to form SiC whiskers in a high-temperature and reducing atmosphere, as confirmed from Fig. 6b.

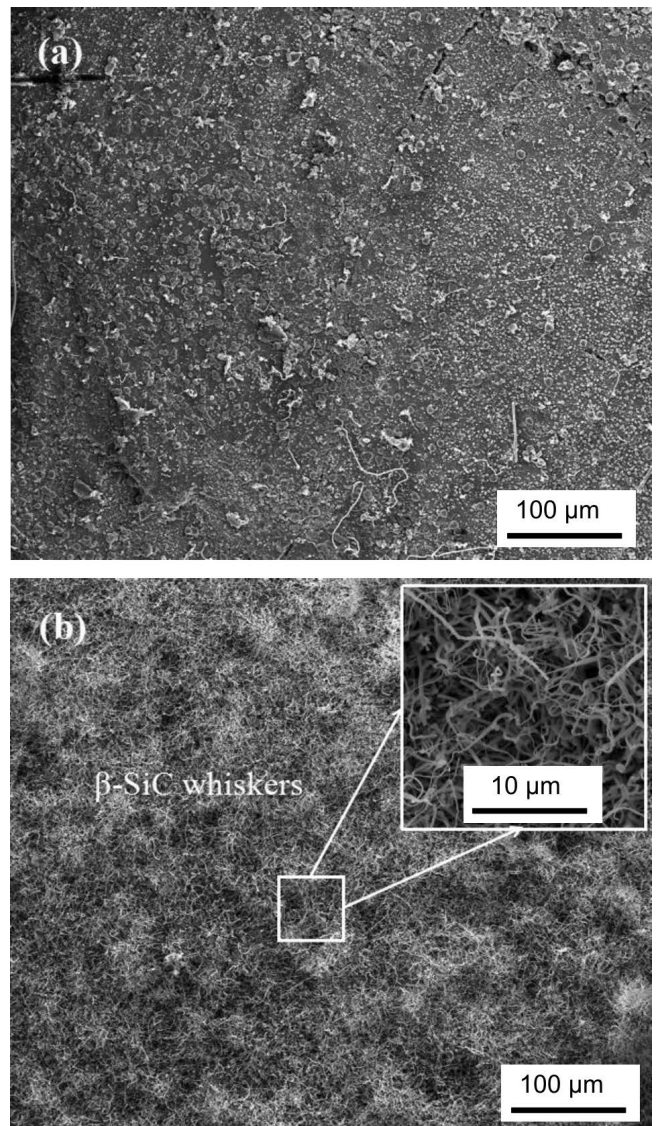


Fig. 6: SEM micrographs of the anthracites fired at 1473 K (1200 °C) with silicon: (a) ECA 5–3 mm, (b) TOA 5–3 mm.

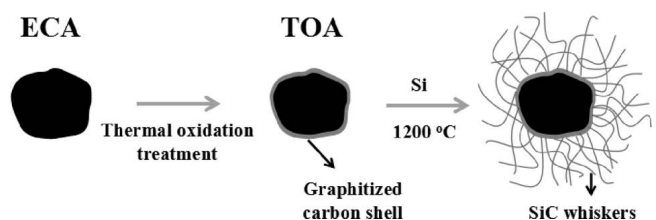


Fig. 7: Schematic illustration for evolution of ECA with silicon after thermal oxidation treatment.

IV. Conclusions

The following conclusions could be made on the basis of the phase composition, microstructure and properties of carbon block refractories fired at 1400 °C in a coke bed.

(1) The properties of carbon block refractories were influenced by the addition of thermally oxidized anthracite (TOA). The TOA accelerated the *in-situ* formation of ceramic phases in specimens because of its higher reactivity than electrically calcined anthracite, thus enhancing the properties of carbon block refractories.

(2) The location of the ceramic whiskers was strongly dependent on the TOA raw materials and different matrix structure led to different properties. With addition of TOA powder, the ceramic whiskers formed in the matrix, which were more favorable for forming an excellent microporosity structure as these filled the pores. With addition of TOA aggregates, on the other hand, the ceramic whiskers mainly appeared on the aggregates, which were more beneficial for reducing the interface thermal resistance between the aggregates and the matrix and subsequently promoted the thermal conductivity of carbon block refractories.

Acknowledgments

The authors appreciate the financial support from the National Natural Science Foundation of China (51574186).

References

- Zhang, G.L., Ma, L.Q., Xiang, Z.L., Zhang, J.P.: Selection of materials and property of carbon blocks for blast furnace, *Carbon Techniques*, **6**, 44–47, (2003).
- Liu, Z.J., Zhang, J.L., Zuo, H.B., Yang, T.J.: Recent progress on long service life design of Chinese blast furnace hearth, *ISIJ International*, **52**, 1713–1723, (2012).
- Li, Y.W.: Optimization of microstructure and performance of refractories for blast furnace hearth. 2014, PhD Dissertation, Wuhan University of Science and Technology.
- Jiao, K.X., Zhang, J.L., Liu, Z.J., Xu, M., Liu, F.: Formation mechanism of the protective layer in a blast furnace hearth. *Int. J. Min., Met. Mater.*, **52**, 1713–1723, (2012).
- Hao, Y.Z., Hao, Q.: Selection of local supplied material for blast furnace bottom and hearth lining and lining structure, *Ironmaking*, **24**, 39–42, (2005).
- Chen, X.L., Li, Y.W., Li, Y.B., Jin, S.L., Zhao, L., Ge, S.: Effect of temperature on the properties and microstructures of carbon block refractories for blast furnace, *Metall. Mater. Trans. A*, **40**, 1675–1683, (2009).
- Li, Y.W., Chen, X.L., Sang, S.B., Li, Y.B., Jin, S.L., Zhao, L., Ge, S.: Microstructures and properties of carbon block refractories for blast furnaces with SiO₂ and Al additions, *Metall. Mater. Trans. A*, **41**, 2085–2091, (2010).
- Chen, X.L., Li, Y.W., Sang, S.B., Zhao, L., Jin, S.L., Li, S.J.: Properties and microstructures of blast furnace carbon block refractories with Al additions, *Ironmak. Steelmak.*, **37**, 398–405, (2010).
- Li, Y.W., Chen, X.L., Li, Y.B., Jin, S.L., Ge, S., Zhao, L., Li, S.J.: Effect of silicon addition on pore structure and thermal conductivity of fired carbon specimens, *Naihuo Cailiao*, **42**, 401–404, (2008).
- Chen, X.L., Li, Y.W., Li, Y.B., Jin, S.L., Ge, S., Zhao, L., Li, S.J.: Effect of silicon particle size on porous structure and thermal conductivity of coked carbon brick, *J. Wuban Univ. Sci. Technol.*, **32**, 155–159, (2009).
- Liao, N., Li, Y.W., Jin, S.L., Xu, Y.B., Sang, S.B., Deng, Z.J.: Combined effects of boron carbide, silicon, and MWCNTs in alumina-carbon block refractories on their microstructural evolution, *J. Am. Ceram. Soc.*, 2016, doi: <https://doi.org/10.1111/jace.14543>.
- Li, Y.W., Sang, S.B., Li, Y.W.: *In-situ* decomposition of kyanite and its influence on properties of carbon blocks, *Bull. Chin. Ceram. Soc.*, **34**, 938–950, (2015).
- Zhu, T.B., Li, Y.W., Sang, S.B., Chen, X.L., Zhao, L., Li, Y.B., Li, S.J.: Microstructure and properties of zircon-added carbon block refractories for blast furnace, *Metall. Mater. Trans. A*, **43**, 4356–4363, (2012).
- Roungos, V., Aneziris, C.G.: Improved thermal shock performance of Al₂O₃-C refractories due to nanoscaled additives, *Ceram. Int.*, **38**, 919–927, (2012).
- Kun, P., Tapasztó, O., Weber, F., Balazsi, C.: Determination of structural and mechanical properties of multilayer graphene added silicon nitride-based composites, *Ceram. Int.*, **38**, 211–216, (2012).
- Luo, M., Li, Y.W., Jin, S.L., Sang, S.B., Zhao, L., Li, Y.B.: Microstructures and mechanical properties of Al₂O₃-C refractories with addition of multi-walled carbon nanotubes, *Mater. Sci. Eng., A*, **548**, 134–141, (2012).
- Li, Y.W., Chen, X.L., Li, Y.B., Sang, S.B., Zhao, L.: Effect of multiwalled carbon nanotubes on the thermal conductivity and porosity characteristics of blast furnace carbon block refractories, *Metall. Mater. Trans. A*, **41**, 2383–2387, (2010).
- Wang, Q.H., Li, Y.W., Sang, S.B., Jin, S.L.: Effect of the reactivity and porous structure of expanded graphite (EG) on microstructure and properties of Al₂O₃-C refractories, *J. Alloy. Compd.*, **645**, 388–397, (2015).
- Zhu, T.B., Li, Y.W., Jin, S.L., Sang, S.B. et al.: Microstructure and mechanical properties of MgO-C refractories containing expanded graphite, *Ceram. Int.*, **39**, 4529–4537, (2012).
- Zhu, T.B., Li, Y.W., Luo, M., Sang, S.B. et al.: Microstructure and mechanical properties of MgO-C refractories containing graphite oxide nanosheets (GONs), *Ceram. Int.*, **39**, 3017–3025, (2012).
- Gonzalez, D., Montesmorán, M.A., Suarez-Ruiz, I., Garcia, A.B.: Structural characterization of graphite materials prepared from anthracites of different characteristics: A comparative analysis, *Energy Fuels*, **18**, 365–370, (2004).
- Gonzalez, D., Montesmorán, M.A., Garcia, A.B.: Graphite materials prepared from an anthracite: A structural characterization, *Energy Fuels*, **17**, 1324–1329, (2003).
- Atria, J.V., Rusinko, F., Schobert, H.H.: Structural ordering of pennsylvania anthracites on heat treatment to 2000–2900 °C, *Energy Fuels*, **16**, 1343–1347, (2002).
- Gonzalez, D., Altin, O., Eser, S., Garcia, A.B.: Temperature-programmed oxidation studies of carbon materials prepared from anthracites by high temperature treatment, *Mater. Chem. Phys.*, **101**, 137–141, (2007).
- Li, Y.W., Wang, Q.H., Fan, H.B., Sang, S.B., Li, Y.B., Zhao, L.: Synthesis of silicon carbide whiskers using reactive graphite as template, *Ceram. Int.*, **40**, 1481–1488, (2014).
- Wang, T.S., Li, Y.W., Sang, S.B.: Nickel-catalyzed construction of heat conductive network in electrically calcined anthracite (ECA) based carbon blocks, *China's Refractories*, **26**, 31–37, (2017).
- Wang, Y., Alsmeyer, D.C., McCreery, R.L.: Raman spectroscopy of carbon materials: Structural basis of observed spectra, *Chem. Mater.*, **2**, 557–563, (1990).
- Illekova, E., Csomorova, K.: Kinetics of oxidation in various forms of carbon, *J. Therm. Anal. Calorim.*, **80**, 103–108, (2005).
- Sharma, H.N., Pahalagedara, L., Joshi, A., Suib, S.L., Mhadeshwar, A.B.: Experimental study of carbon black and diesel engine soot oxidation kinetics using thermogravimetric analysis, *Energy Fuels*, **26**, 5613–5625, (2012).
- Menendez, J.A., Arenillas, A., Fidalgo, B., Fernandez, Y., Zubizarreta, L., Calvo, E.G., Bermudez, J.M.: Microwave heating processes involving carbon materials, *Fuel Process. Technol.*, **91**, 1–8, (2010).

